### Title

Cerenkov light transport in scintillation crystals explained: realistic simulation with GATE




### Journal

Biomedical Physics & Engineering Express, 5(3)

### ISSN

2057-1976



### Authors

Roncali, Emilie
Kwon, Sun Il
Jan, Sebastien
et al.



### Publication Date

2019-04-01

### DOI

10.1088/2057-1976/ab0f93

Peer reviewed

HHS Public Access

Author manuscript

*Biomed Phys Eng Express*. Author manuscript; available in PMC 2020 December 09.

Published in final edited form as:

*Biomed Phys Eng Express*. 2019 April ; 5(3): . doi:10.1088/2057-1976/ab0f93.

# Cerenkov light transport in scintillation crystals explained: realistic simulation with GATE

**Emilie Roncali**[1], **Sun Il Kwon**[1], **Sebastien Jan**[2], **Eric Berg**[1], **Simon R Cherry**[1]

[1]Department of Biomedical Engineering, University of California, Davis, One Shields Avenue, Davis, CA 95616, United States of America

[2]IMIV, CEA, Inserm, CNRS, Univ. Paris-Sud, Université Paris Saclay, CEA-SHFJ, 91 400, Orsay, France

## Abstract

**Purpose:** We are investigating the use of promptly emitted Cerenkov photons to improve scintillation detector timing resolution for time-of-flight (TOF) positron emission tomography (PET). Bismuth germanate (BGO) scintillator was used in most commercial PET scanners until the emergence of lutetium oxyorthosilicate, which allowed for TOF PET by triggering on the fast and bright scintillation signal. Yet BGO is also a candidate to generate fast timing triggers based on Cerenkov light produced in the first few picoseconds following a gamma interaction. Triggering on the Cerenkov light produces excellent timing resolution in BGO but is complicated by the very low number of photons produced. A better understanding of the transport and collection of Cerenkov photons is needed to optimize their use for effective triggering of the detectors.

**Methods:** We simultaneously generated and tracked Cerenkov and scintillation photons with a new model of light transport that we have released in GATE V8.0. This crystal reflectance model was used to study photon detection and timing properties, building realistic waveforms as measured with silicon photomultipliers.

**Results:** We compared the behavior and effect of detecting Cerenkov and scintillation photons at several levels, including detection time stamps, travel time, and coincidence resolving time in 3 × 3 × 20 $mm^3$ BGO crystals. Simulations showed excellent agreement with experimental results and indicated that Cerenkov photons constitute the majority of the signal rising edge. They are therefore critical to provide early triggering and improved the coincidence timing resolution by 50%.

**Potential applications:** To our knowledge, this is the first complete simulation of the generation, transport, and detection of the combination of Cerenkov and scintillation photons for TOF detectors. This simulation framework will allow for quantitative study of the factors influencing timing resolution, including the photodetector characteristics, and ultimately aid the development of BGO and other Cerenkov-based detectors for TOF PET.

### Keywords

Cerenkov; timing resolution; positron emission tomography; radiation detector; Monte Carlo simulation

## 1. Introduction

While most positron emission tomography scanners (PET) in the 1990s employed bismuth germanate (BGO) scintillation crystals, lutetium oxyorthosilicate (LSO) and the closely related lutetium yttrium oxyorthosilicate (LYSO) rapidly became the scintillator of choice following their development in the mid-1990s (Melcher and Schweitzer 1992). LSO and LYSO offered several advantages including improved energy resolution and timing resolution suitable for time-of-flight (TOF) PET (Melcher and Schweitzer 1992, Moses et al 2010). The benefit of including TOF in reconstruction algorithms to improve image contrast has been demonstrated by multiple groups (Karp et al 2008, Conti 2009, Moses et al 2010) and was explored in the 1980s (Budinger 1983), but was not widely adopted at that time because of the limitations in available scintillators and electronics. In particular, BGO was deemed unsuitable for TOF PET, because of its low light yield and slow decay time (Melcher 2000). Following the huge progress in improving coincidence timing resolution, which has now reached 250–400 ps in commercial PET scanners, there is an interest to achieve ultra-fast timing resolution using prompt sources of luminescence to overcome the statistical limits of triggering on the relatively slowly emitted scintillation light (tens of nanoseconds). Thanks to its high refractive index (2.15 at 480 nm) and high transparency for UV-blue light, BGO is an excellent candidate to emit Cerenkov light produced by energetic electrons resulting from a photoelectric or Compton interaction, over an extremely short time frame of about 10 ps (Williams et al 1996, Williams et al 2001). Triggering detectors on Cerenkov emission to achieve superior timing resolution has been investigated in recent years (Lecoq 2012, Somlai-Schweiger and Ziegler 2015) and its feasibility in BGO crystals has been demonstrated by several studies (Kwon et al 2016a, Brunner and Schaart 2017b, Cates et al 2018). These studies also highlighted the challenges associated with time triggering based on the very few Cerenkov photons produced per photoelectric interaction (~15–20 per 511 keV photoelectric interaction in BGO) and indicated that more detailed understanding of the light transport in the crystal and collection by the photodetector is needed to optimize the use of Cerenkov photons for timing.

In this work, we use advanced optical Monte Carlo simulation to study the transport and detection of Cerenkov light. We simultaneously generate and track both Cerenkov and scintillation photons with GATE, using a new model of light transport in crystals that we have recently released in GATE (Stockhoff et al 2017). This crystal reflectance model allows for accurate description of the light propagation in the scintillator, combining the measured topography of the crystal and a detailed model of the reflector to describe the reflectance and transmittance of the crystal surface (Roncali et al 2017). The choice of surface finish, reflector, and photodetector can alter the detection and timing properties of optical photons and can improve the collection (by maximizing the detection probability) and timing of the Cerenkov photons (by minimizing the travel time in the crystal). The distribution of photon detection times, or time stamps, defines the light pulse resulting from each gamma interaction in the crystal and has contributions from both scintillation and Cerenkov photons. The ability to simultaneously study Cerenkov and scintillation photons is critical because their mixing in the light pulse influences the timing performance. By measuring the entire waveform of each interaction, the overall shape and timing properties of the light pulses can

be studied; however the respective contributions of Cerenkov and scintillation photons cannot be directly measured experimentally and can only be studied by conducting simulations where both types of optical photons are generated.

To produce realistic simulated light pulses with the shape of measured waveforms, the distribution of detection times is combined with a model of the photodetector (PD) coupled to the crystal front or back face. Here we use a model of a silicon photomultiplier (SiPM) that we have developed and parameterized to represent the SiPMs we used in previous experimental studies (Kwon et al 2016a). We compare the effect of the photodetector position on timing resolution to our experimental results.

We demonstrate the feasibility of the complete simulation of Cerenkov and scintillation photons from generation to detection and apply it to the study of timing performance of BGO detectors. Results demonstrated that simulations can support experimental studies by explaining the observed phenomena. To our knowledge, this is the first complete simulation of the generation, transport, and detection of Cerenkov photons in the context of TOF PET detectors.

## 2. Materials and methods

### 2.1. Generation of Cerenkov and scintillation photons in GATE V8.0

**2.1.1. Generation of scintillation photons—**All GATE simulations were conducted in BGO crystals. BGO optical properties were defined by an isotropic emission following a single exponential decay with a time constant of 300 ns, a broad emission spectrum with a peak at 480 nm, and an index of refraction varying from 2.36 at 320 nm to 2.07 at 800 nm (Williams et al 1996). As the number of Cerenkov photons produced in a material depends on the index of refraction according to the Frank-Tamm formula (Jelley 1955), the wavelength dependency will affect the Cerenkov yield and must be modelled. BGO also has a fast decay component of 60 ns that represents only 10% of the emission and was not modelled in these simulations (Moszyñski et al 1981). Because of the lack of reliable measurement of the BGO rise time, which has been reported as fast as 30 ± 30 ps (Derenzo et al 2000) and as slow as 2.8 ns (Moszyñski et al 1981, Anderson 1989), it was not included in these studies. Using a rise time value longer than real would delay the production of scintillation photons and would give a stronger weight to the contribution of Cerenkov photons to early triggering, which would not be representative of the actual detector.

Finally, the absorption length is shorter at lower wavelengths where Cerenkov photons are mostly emitted, which will reduce their transmission (figure 1) (Wenzel 2010). This effect was modelled in this work.

**2.1.2. Generation of Cerenkov photons—**The generation of the Cerenkov photons in GATE is based on the physics models implemented in Geant4. Following a 511 keV interaction in the crystal, secondary electrons are emitted non-isotropically, such that their initial trajectories are mostly in the forward direction with respect to the path of the incident 511 keV photon. Along the path of an energetic secondary electron, Cerenkov photons maybe emitted with directions determined by the kinetic energy and momentum of the

electron, and the index of refraction of the medium (Jelley 1955). The initial Cerenkov photons are therefore mostly emitted in a forward direction, as opposed to scintillation photons which are emitted isotropically. Each Cerenkov photon, similarly to scintillation photons, is reflected on the faces of the crystal as shown in blue in figure 2 until it is detected (green dot), or transmitted through the sides, or absorbed in the bulk material. The reflection probability depends on the reflectance and transmittance properties of the crystal surfaces, while the probability of absorption depends on the attenuation length (figure 1(c)). Forward photons are defined as photons travelling toward the photodetector (or in the same direction as the incident gamma photon), while backward photons are travelling in the opposite direction (Kwon and R C S 2017).

## 2.2. Transport of optical photons in GATE V8.0

**2.2.1. Reflectance and transmittance model—**All simulations were conducted using the LUT Davis model implemented in GATE V8.0 (Stockhoff et al 2017). This model relies on a high resolution measured crystal topography (typically obtained from 100 nm resolution atomic force microscopy scans) combined with a model of the reflector or paint attached to the crystal surface, and has been shown to accurately describe polished or rough surfaces (Roncali et al 2017). The model takes into account multiple reflections between the crystal and the outer material to compute reflectance and transmittance look-up-tables (LUTs) called every time a photon interacts with the crystal boundaries. Depending on the angle of incidence of that optical photon, the LUTs determine whether the photon is transmitted or reflected, and in which direction. Here, LUTs describing polished surfaces were used to study the Cerenkov and scintillation photon transport. All five faces of the crystal that were not in contact with the photodetector were modelled with the same optical properties, e.g. all polished with or without reflector. The reflector was modelled as Teflon tape, with an air interface between the reflector and crystal. The commonly used specular reflector ESR was not considered in our simulations because it has poor transmission in the Cerenkov emission range (Park 2012) and is therefore expected to degrade the light collection compared to Teflon. The crystal face coupled to the photodetector was modelled as a polished surface in contact with a coupling material (e.g. optical grease, index of refraction 1.5) for all simulations.

**2.2.2. Transport of Cerenkov and scintillation photons in the crystal—**All detected photons were saved in ROOT in listmode (Brun and Rademakers 1997). Each photon has several ID numbers recorded during the simulation that allowed us to identify its parent electron and ultimately the gamma event from which the electron originated is identified. Subsequently, all photons originating from the same gamma event are grouped. Multiple characteristics of each photon's life and fate were saved, such as detection time, travel time in the crystal, 3D coordinates of the final position and momentum, and energy. The detection time is the sum of the emission time (after interaction) and travel time in the crystal.

Detected photons were defined as photons that crossed the interface between the crystal and the photodetector and did not include photons absorbed in the bulk of the crystal. The coupling material between the crystal and photodetector was modelled with a refractive

index of 1.5, and 100% transparency for Cerenkov and scintillation photons. For this section only, the photodetector geometric detection efficiency and photodetection efficiency (PDE) was considered perfect (=1). Lastly, the GATE source code was modified to add a variable to discriminate Cerenkov photons from scintillation photons.

### 2.3. Simulation of coincidence timing spectra

Each detected optical photon carries a detection time defined as the time it crossed the crystal-photodetector interface. For each gamma interaction, the photon detection times were histogrammed to build a light pulse, which was then convolved with the single photon response of the NUV-HD SiPM developed by FBK (Piemonte et al 2016) and used in our previous experiments. The SiPM has a cell pitch of 40 $\mu$m, a fill factor of 83%, and a total sensitive area of $4 \times 4$ mm$^2$. The PDE of the NUV-HD SiPM was modelled as over 45% between 300 nm and 400 nm, and peaks at 400–420 nm with a maximum value of 60% at 10.3 V overvoltage (Kwon et al 2016a). A dark count rate of 350 kHz and an optical cross-talk probability of 70% were used to add noise to the waveforms before performing timing pick-off. Timing pick-off for each waveform was defined as the time where the leading edge of the waveform crossed a set threshold. The SiPM time response was modelled as a dual-exponential with a rise time of 4 ns and decay time of 20 ns. The transit time spread of the SiPM was modelled through a Gaussian distribution with a full width half maximum of 90 ps (Piemonte and Gola 2018). Timing pick-off values were obtained for a range of thresholds and the best timing resolution was retained. The timing spectra were computed by subtracting timing pick-off values from each detector and histogramming the differences. The shape of the timing spectra, which is not well described by a Gaussian distribution according to our previous experimental work, was carefully studied for scintillation photons only and scintillation + Cerenkov photons.

### 2.4. Simulation parameters and configurations

Simulations were conducted with a 511 keV monoenergetic, back-to-back source located at equal distance from each detector composed of a $3 \times 3 \times 20$ mm$^3$ BGO crystal coupled to NUV-HD SiPM. A total of 7000–10 000 events were collected in each detector depending on the configurations. Arrangements with the photodetector placed in front or at the back of the crystal were compared (figure 3, table 1).

The same configurations were used to acquire coincidence events from a $^{22}$Na point source, as described in (Kwon et al 2016a). The energy and timing output were filtered with a pole-zero cancellation circuit and were digitized with a high-performance oscilloscope (DPO71254C, Tektronix) at a sampling rate of 50 GS s$^{-1}$ (20 ps time bin) and a bandwidth of 3 GHz. Coincidence events within the FWTM around the 511-keV photopeak were used for timing analysis. The time pick-off of each timing signal was determined by leading edge thresholding after linear interpolation, similarly to the simulations.

# 3. Results

## 3.1. Light collection

**3.1.1. Emitted and detected Cerenkov photons—**We studied the number of Cerenkov emitted per gamma event and the corresponding number of detected photons. For 10 000 photoelectric interactions at 511 keV (i.e. excluding Compton events) in BGO, the number of emitted Cerenkov and detected photons was histogrammed and fitted with a Gaussian distribution to extract the mean values (figure 4). For photoelectric interactions, the mean number of emitted photons was 17.9, which is consistent with other simulations (Brunner et al 2014, Kwon and R C S 2017). The number of emitted photons can be described by the Frank-Tamm formula and entirely depends on the radionuclide source and the bulk properties of the scintillator such as the number of secondary electrons created by a gamma interaction, the electron velocity, and the index of refraction of the material (Jelley 1955). However, the number of photons reaching the photodetector (labelled as 'detected' in this section) is also determined by the light transport in the crystal. Except for the bulk absorption, the major characteristics are related to the reflection of the light on the crystal boundaries and will vary depending on the crystal aspect ratio, surface treatment, and attached reflector. For a polished crystal wrapped in Teflon tape, only 3.4 Cerenkov photons on average were detected per 511 keV photoelectric interaction, which represents 18% of the emitted photons (figure 4). When including fully deposited (i.e. not escaped) Compton events, the number of Cerenkov photons detected per interaction dropped to 2.22. Figure 5 shows the number of detected Cerenkov photons per 511 keV interaction (photoelectric events plus Compton events with full energy deposition) for all configurations described in figure 3.

With the photodetector placed in front of the crystal wrapped in Teflon, as shown in figure 3, we calculated that 1.74 Cerenkov photons would be detected, which is less than the 2.22 detected photons when the photodetector is at the back of the crystal. In contrast, more scintillation photons were detected in the front configuration (565 instead of 469). Because of the gamma attenuation length of BGO, gamma interactions on average occur closer to the photodetector when it is placed in front, which explains why the isotropically-emitted scintillation light can be more efficiently collected in this configuration. In contrast, the earliest Cerenkov photons are emitted in a forward direction and tend to travel to the end of the crystal opposite to the entrance face, which explains why fewer photons are collected when the photodetector is placed in front, i.e. on the entrance face.

**3.1.2. Number of reflections—**For detected optical photons, the number of reflections on the crystal boundaries was recorded and histogrammed. Figure 6 shows the comparison between Cerenkov and scintillation photons. Because the number of Cerenkov photons is much lower than that of scintillation photons, the histograms were normalized to contain the same number of photons. While the peak position is very similar at 3–4 reflections per photon, the tail drastically changes, with scintillation photons undergoing many more reflections (blue curve). The first peak (with less than 15 reflections per photon) corresponding to the forward propagating photons represents 90% of emitted Cerenkov photons and only 42% of emitted scintillation photons. This difference is related to (1) the

non-isotropic emission of Cerenkov photons, and (2) the greater attenuation of Cerenkov photons (see figure 1(c)). Cerenkov photons are predominantly emitted in the 'forward' direction with respect to the incident gamma photon direction and are therefore detected after a lower number of reflections (Kwon and R C S 2017) Scintillation photons are emitted isotropically, and may undergo more reflections before being detected, which will lengthen the travel time in the crystal and detection time.

### 3.2. Travel time in the crystal

We studied the travel time in the crystal for both back and front photodetector (PD) configurations. The travel times of photons emitted following a gamma interaction at a depth-of-interaction of 2 ± 0.1 mm and 18 ± 0.1 mm (DOI) were histogrammed separately for Cerenkov emission and scintillation with time bins of 5 ps. Figure 7 shows the histograms normalized by the number of gamma events. Because the scintillation emission is isotropic and the two DOI positions are at equal distance from the photodetector face, the front PD should detect scintillation photons from DOI 2 mm the same way the Back PD detects scintillation photons from DOI 18 mm. This is confirmed by figures 7(b) and (d) which both show one curve with a sharp peak starting at 15 ps corresponding to forward-emitted photons traveling the shortest distance between the DOI and the photodetector face (i.e. 2 mm), and a second peak starting at 275 ps corresponding to the minimum distance of 38 mm travelled by backward-emitted photons. When the selected DOI is 18 mm away from the photodetector, the forward and backward peaks are overlapping, with a rising edge starting at 129 ps (corresponding to 18 mm) and a rising edge of 175 ps (corresponding to 22 mm to travel back and forth). In contrast, we hypothesized that the back PD configuration is more favourable to detect Cerenkov photons because they are predominantly emitted forward and need an additional reflection by the back face to reach the Front PD. Results from figures 7(a) and (c) support this hypothesis, with a forward peak 40% larger for the Back PD configuration (dash versus solid lines). This is also supported by the results at DOI 18 mm showing that the forward peak rises slightly earlier for the Back PD configuration.

### 3.3. Detection time

Photon detection times are defined as the time stamps when they crossed the crystal-photodetector interface and include the gamma travel time, the emission time, and the optical travel time. For scintillation photons, the emission is a slow exponential decay process with a time constant of 300 ns and is the dominating factor in the detection time rather than the very short travel time. Since the emission time is independent of the surface treatment no changes were observed with roughening or the addition of a reflector. In contrast, the Cerenkov emission is shorter than the travel time itself. As a result, the Cerenkov detection times match the travel times well (figure 8(a)). Similar to figure 7, the first peak corresponds to forward-emitted photons traveling a minimum distance of 10 mm and the second peak corresponds to backward-emitted photons traveling at least 30 mm. Figure 8(b) shows the number of detected photons in 10 ps time bins. It shows that the Cerenkov detection times are < 1 ns, even when looking at all DOIs combined for a polished crystal wrapped in Teflon. 99% of Cerenkov photons were detected in 600 ps, whereas only 0.1% of the scintillation photons were detected in that time frame. Here the BGO scintillation was modelled without rise time; adding it would slow down the initial emission

rate and thus further decrease the number of scintillation photons emitted and detected in the first 600 ps. This implies that early triggering primarily depends upon Cerenkov photons and confirms their importance for fast timing resolution.

Figure 8(b) also shows the distribution of the first detected Cerenkov photon detection times per gamma interaction, in 10 ps time bins (dashed red line). Note that the first detected photon is not necessarily the first emitted photon, which may have been lost through the sides of the crystal or absorbed. The distribution is narrower than when looking at all Cerenkov photons, indicating the interest of being able to trigger on this first detected photon.

### 3.4. Realistic waveforms with a NUV-HD SiPM model

**3.4.1. Effect of Cerenkov photons on waveform and timing pickoff—**After studying the detection times and travel times of the photons, we now build realistic waveforms by convolving the detection time distributions with the SiPM response, modelling the NUV-RGB SiPM described in section 2.3. An example of a waveform for a given gamma interaction is shown in figure 9(a) (green curve). Simulated data allow us to separate the scintillation from the Cerenkov photons and build the waveform for scintillation photons only and Cerenkov photons only (blue and red curves). As shown in figure 8(b), the Cerenkov photons primarily affect the rising edge of the signal (see also inset in figure 9(a)) by making it shorter and would be the primary trigger when using a leading edge discriminator with a low threshold, indicated by the dashed line. In this example, the pickoff time would increase from ~230 ps to ~1.7 ns if only scintillation photons were considered. This is reflected in the distribution of the pickoff times (figure 9(b)). The distribution of the total waveform (including Cerenkov photons) has an earlier peak but most importantly for timing resolution is much narrower, suggesting that the timing spectrum will be narrower as well and leading to improved timing resolution. Figure 9(b) also shows that when the photodetector is the back of the crystal, the distribution of pickoff times including Cerenkov and scintillation photons is slightly narrower than when the photodetector is placed in the front, which suggests that the CRT may be improved.

**3.4.2. Effect of Cerenkov photons on timing spectrum and CRT—**Timing spectra were built from the pickoff times for different configurations. One of the primary goals was to explain the non-Gaussian shape that our and others' experimental studies showed (Kwon et al 2016a, Brunner and Schaart 2017b). The timing spectrum obtained for a polished crystal wrapped in Teflon with the photodetector in the back was first fitted with a Gaussian distribution which clearly does not reflect the tails of the distribution (figure 10). In contrast, the Lorentz function provided a much better fit, which is consistent with findings from Kwon et al (Kwon et al 2016a). The full width half maximum (FWHM) extracted from the Gaussian and Lorentzian fits are 441 ps and 420 ps, respectively. The main difference is observed in the full width tenth maximum (FWTM), which is much closer to the data when fitting with a Lorentzian distribution (804 ps, 1180 ps, and 1220 ps for the Gaussian fit, Lorentzian, and data respectively).

The coincidence resolving time (CRT) extracted from Gaussian fits are given in table 2 for crystals wrapped in Teflon with photodetector in the back or front. Although we demonstrated that a Lorentzian is more adapted to the timing spectra, the choice of the traditional Gaussian fit and FWHM CRT allows us to compare our findings to other works. Consistent with experimental studies from Kwon et al (Kwon et al 2016a), the timing resolution degraded when the photodetector was placed in front of the BGO crystal. This can be explained by the lower number of detected Cerenkov photons in this configuration (1.74 instead of 2.21 per 511 keV interaction) that results in poorer timing pick-off and ultimately in poorer timing resolution. Here an increase of 71 ps was measured between the back-to-back and front-to-front configurations for a CRT of 441 ps. This is in reasonable agreement with our experimental results that showed a CRT of 455 ps with a back-to-back configuration (figure 10(b)) and a degradation of 138 ps in front-to-front. when placing the photodetector in front of the crystal. In contrast, the CRT slightly improves in the front-to-front configuration when considering only scintillation photons (649 ps to 607 ps FWHM), which is consistent with the larger number of scintillation photons collected in this configuration (565 instead of 469).

The benefit of Cerenkov photons for timing resolution is demonstrated by the CRT values: if only scintillation photons were considered, the CRT would degrade by 50%.

## 4. Discussion

The major goal of this simulation study is to explain the transport of scintillation and Cerenkov photons in BGO crystals and to demonstrate the development of a simulation tool that can be used to optimize Cerenkov-based scintillation detectors for time-of-flight PET. Simulations were conducted with a look-up-table approach to model the crystal surface treatment and reflector, a critical point in Monte Carlo simulations of such detectors. Simulations allowed for the separation of scintillation and Cerenkov photons, providing a unique understanding of the light transport of each type of light photons involved in these BGO detectors that is impossible to fully extract using a purely experimental approach.

The separation of Cerenkov and scintillation photons in the simulations revealed differences in light transport in the crystal. The emission time of Cerenkov photons is essentially negligible compared to the transport time, which makes the Cerenkov photon detection times much more sensitive to the transport compared to the scintillation photon detection times. One important finding is that Cerenkov photons constitute most of the early signal and therefore early triggering for timing resolution relies on these photons, as shown in figure 9(b). It is important to note that no scintillation rise time was modelled in these simulations because of the uncertainty of literature values (30 ± 30 ps according to (Moses and Derenzo 1994)); a finite rise time would further decrease the number of scintillation photons emitted early and useful for triggering.

We found good agreement with experimental studies published by our group and others (Kwon et al 2016b, Brunner and Schaart 2017a, Cates et al 2018). In particular, the non-Gaussian shape of the timing spectrum, not commonly observed in other traditional timing methods, was reproduced, suggesting that the simulation accurately modelled the timing

properties of the photons. We also found that placing the photodetector in front of the crystal degraded the timing resolution, which was explained by lower detection of the forward-emitted Cerenkov photons. This explanation is also supported by the opposite trend observed with scintillation photons, as the CRT slightly improves in the front-to-front configuration (table 2). These results are consistent with our experimental results and constitute a strong evidence that simulations can play an important role in providing explanation of observed phenomena and ultimately improving the detector design.

Absolute differences can be easily explained by the uncertainty in the SiPM time response, transit time spread temporal and spatial distribution, and dark count rate (noise) used in the model, as well as the effect of the readout electronics, which was not modelled. A large number of parameters are needed to model the SiPM timing properties, and these are not trivial to match with experimental values, especially because they depend on overvoltage and other experimental conditions. The optimization of the photodetector for Cerenkov light collection and timing is equally important to the design of the crystal but is beyond the scope of this paper.

In conclusion, we have shown the feasibility of using Monte Carlo simulations for simultaneous Cerenkov and scintillation photon generation, tracking and collection. This model is useful to understand the behaviour of prompt Cerenkov photons and optimize their use as a source for fast timing discrimination.

## Acknowledgments

This work was funded by NIH R35 CA197608.

## References

Anderson DF 1989 Properties of the high-density scintillator cerium fluoride IEEE Trans. Nucl. Sci 36 137–40

Brun R and Rademakers F 1997 ROOT—an object oriented data analysis framework Nucl. Instrum. Methods Phys. Res. A 389 81–6

Brunner SE, Gruber L, Marton J, Suzuki K and Hirtl A 2014 Studies on the Cherenkov effect for improved time resolution of TOF-PET IEEE Trans. Nucl. Sci 61 443–47

Brunner S and Schaart D 2017a Enabling cost-effective TOF-PET by exploiting the Cherenkov emission in BGO J. Nucl. Med 58 150

Brunner SE and Schaart D 2017b BGO as a hybrid scintillator/Cherenkov radiator for cost-effective time-of-flight PET Phys. Med. Biol 62 4421–39 [PubMed: 28358722]

Budinger TF 1983 Time-of-flight positron emission tomography: status relative to conventional PET J. Nucl. Med 24 73–8 [PubMed: 6336778]

Cates JW, Gundacker S, Auffray E, Lecoq P and Levin CS 2018 Improved single photon time resolution for analog SiPMs with front end readout that reduces influence of electronic noise Phys. Med. Biol 63 185022 [PubMed: 30129562]

Conti M 2009 State of the art and challenges of time-of-flight PET Phys. Medica 25 1–11

Derenzo SE, Weber MJ, Moses WW and Dujardin C 2000 Measurements of the intrinsic rise times of common inorganic scintillators IEEE Trans. Nucl. Sci 47 860–4

Jelley JV. 1955; Cerenkov radiation and its applications. Br. J. Appl. Phys. 6:227.

Karp JS, Surti S, Daube-Witherspoon ME and Muehllehner G 2008 Benefit of time-of-flight in PET: experimental and clinical results J. Nucl. Med 49 462–70 [PubMed: 18287269]

Kwon SI, Gola A, Ferri A, Piemonte C and Cherry SR 2016a Bismuth germanate coupled to near ultraviolet silicon photomultipliers for time-of-flight PET Phys. Med. Biol 61 L38 [PubMed: 27589153]

Kwon SI, Gola A, Ferri A, Piemonte C and Cherry SR 2016b Bismuth germanate coupled to near ultraviolet silicon photomultipliers for time-of-flight PET Phys. Med. Biol 61 L38–47 [PubMed: 27589153]

Kwon SI and R C S 2017 Simulation study of the generation of cerenkov photons in bismuth germanate for PET IEEE Nuclear Science Symp. and Medical Imaging Conf (Atlanta, GA)

Lecoq P 2012 New approaches to improve timing resolution in scintillators IEEE Trans. Nucl. Sci 59 2313–8

Melcher CL 2000 Scintillation crystals for PET J. Nucl. Med 41 1051–5 [PubMed: 10855634]

Melcher CL and Schweitzer JS 1992 Cerium-doped lutetium oxyorthosilicate—a fast, efficient new scintillator IEEE Trans. Nucl. Sci 39 502–5

Moses WW and Derenzo SE 1994 Design studies for a PET detector module using a pin photodiode to measure depth of interaction IEEE Trans. Nucl. Sci 41 1441–5

Moses WW, Janecek M, Spurrier MA, Szupryczynski P, Choong WS, Melcher CL and Andreaco M 2010 Optimization of a lso-based detector module for time-of-flight PET IEEE Trans. Nucl. Sci 57 1570–6 [PubMed: 21738262]

Moszyñski M, Gresset C, Vacher J and Odru R 1981 Timing properties of BGO scintillator Nucl. Instrum. Methods Phys. Res 188 403–9

Park, H; Optics of Vikuiti Films. 2012.

Piemonte C, Acerbi F, Ferri A, Gola A, Paternoster G, Regazzoni V, Zappala G and Zorzi N 2016 Performance of NUV-HD silicon photomultiplier technology IEEE Trans. Electron Devices 63 1111–6

Piemonte C and Gola A 2018 Overview on the main parameters and technology of modern silicon photomultipliers Nucl. Instrum. Methods Phys. Res. A 926 2–15

Roncali E, Stockhoff M and Cherry SR 2017 An integrated model of scintillator-reflector properties for advanced simulations of optical transport Phys. Med. Biol 62 4811–30 [PubMed: 28398905]

Somlai-Schweiger I and Ziegler SI 2015 Cherencube: concept definition and implementation challenges of a Cherenkovbased detector block for PET Med. Phys 42 1825–35 [PubMed: 25832073]

Stockhoff M, Jan S, Dubois A, Cherry S and Roncali E 2017 Advanced optical simulation of scintillation detectors in gate v8.0: first implementation of a reflectance model based on measured data Phys. Med. Biol 62 L1–8 [PubMed: 28452339]

Wenzel, H; Detailed Simulation of Crystals. 2010.

Williams PA, Rose AH, Lee KS, Conrad DC, Day GW and Hale PD 1996 Optical, thermo-optic, electro-optic, and photoelastic properties of bismuth germanate ($Bi_4Ge_3O_{12}$) Appl. Opt 35 3562–9 [PubMed: 21102749]

Williams RT, Ucer KB and LoPresti JL 2001 In the first instants ultrafast views of radiation effects Radiat. Measur 33 497–502

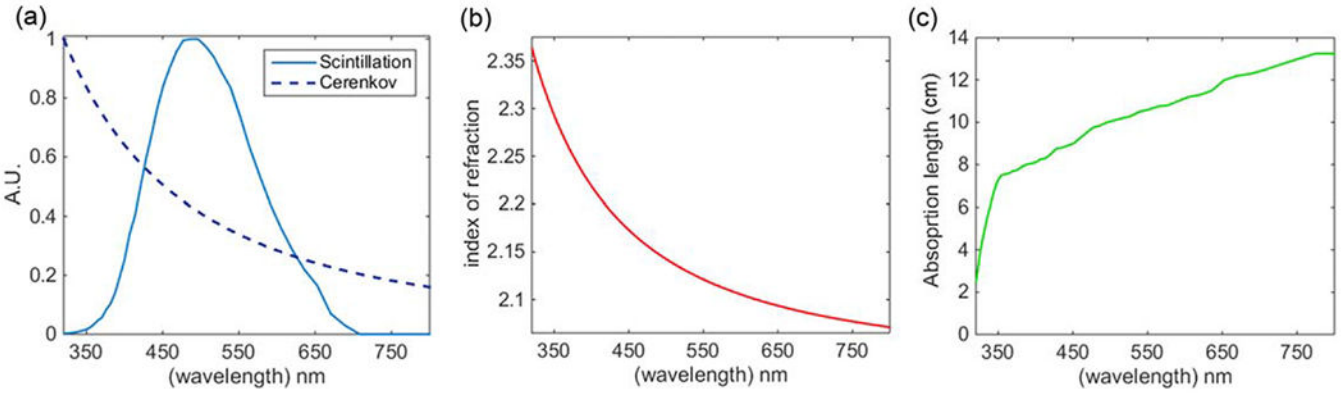


**Figure 1.**

BGO material characteristics. (a) BGO has a broad scintillation emission spectrum with a peak at 480 nm. The Cerenkov emission is inversely proportional to the square of the wavelength. (b) BGO was modelled with a wavelength-dependent index of refraction (from 2.36 to 2.07). (c) The BGO absorption length is shorter at shorter wavelengths where most of the Cerenkov emission occurs.

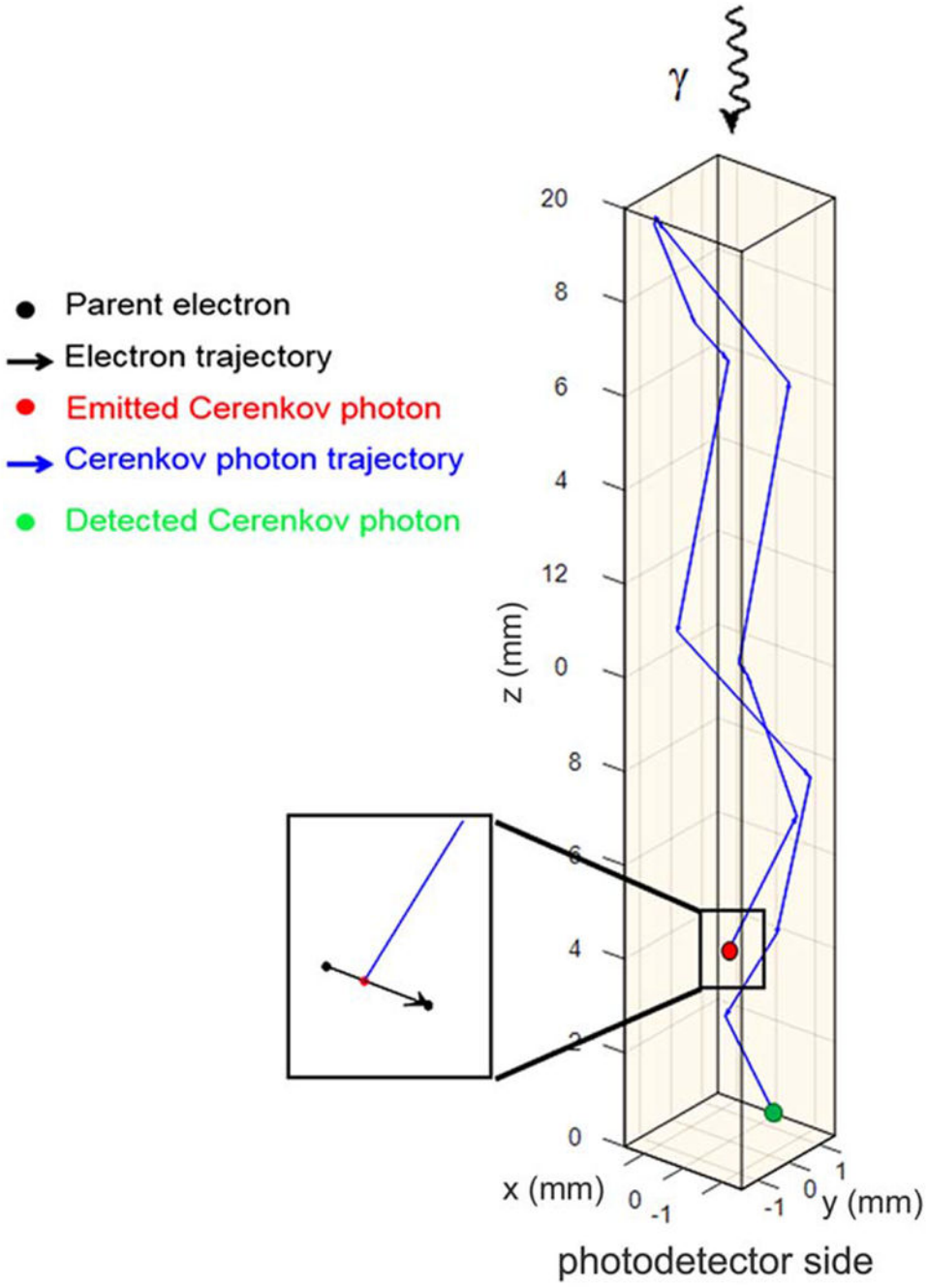


**Figure 2.**

Example of optical transport in a 3 × 3 × 20 $mm^3$ BGO crystal. The inset shows the secondary electron and the emission of a Cerenkov photon (in red) along the electron path. The photon bounces on the faces (in blue) until detection (in green) or loss.

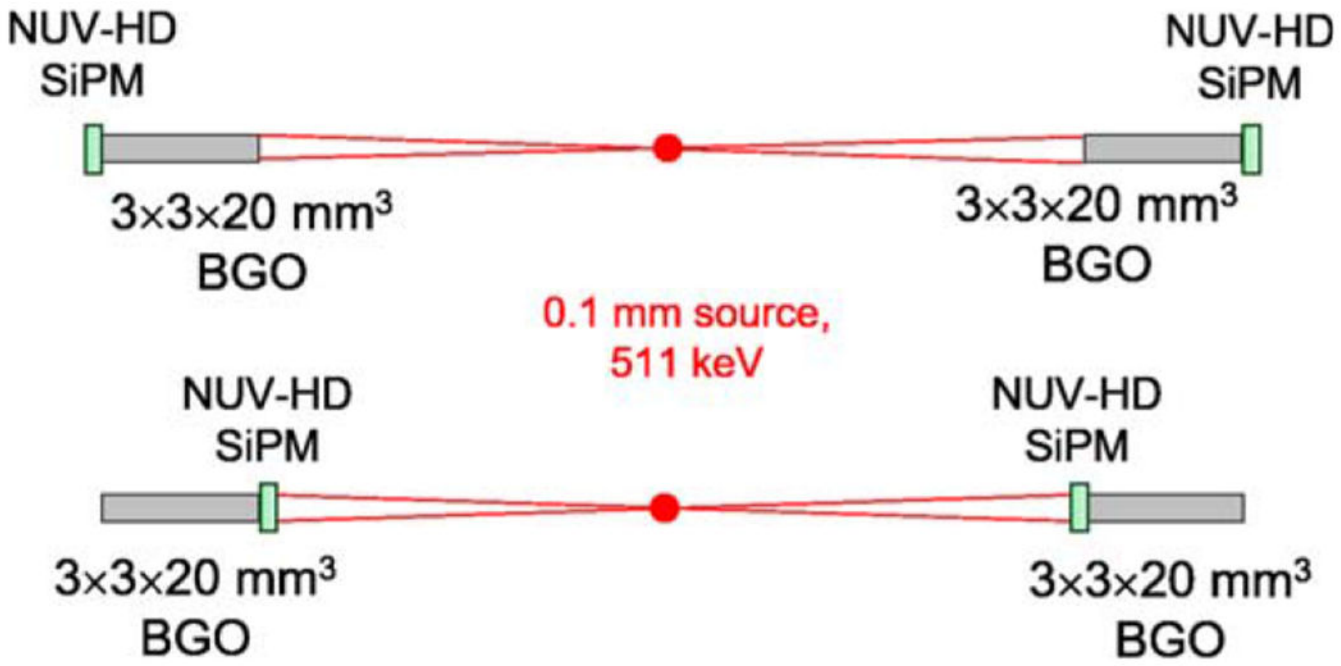


**Figure 3.**

Two geometries were used, each composed of two identical detectors. From top to bottom: 20 mm-long crystal with photodetector in the back (back-to-back), 20 mm-long crystal with photodetector in front (front-to-front).

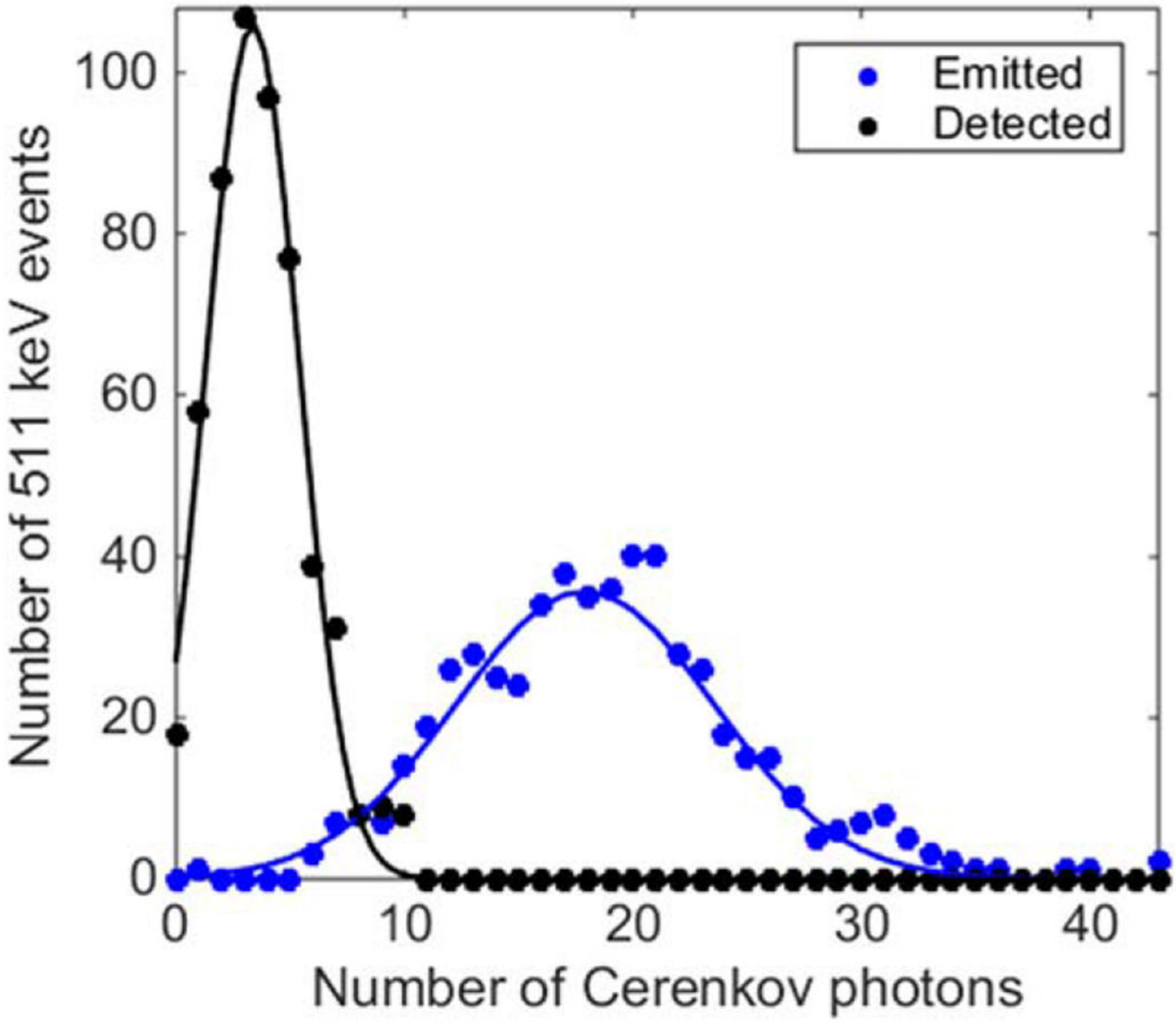


**Figure 4.**
Number of Cerenkov photons emitted and detected per 511 keV photoelectric interaction, in a polished crystal wrapped in Teflon tape. The photodetector was considered ideal (all photons are detected).

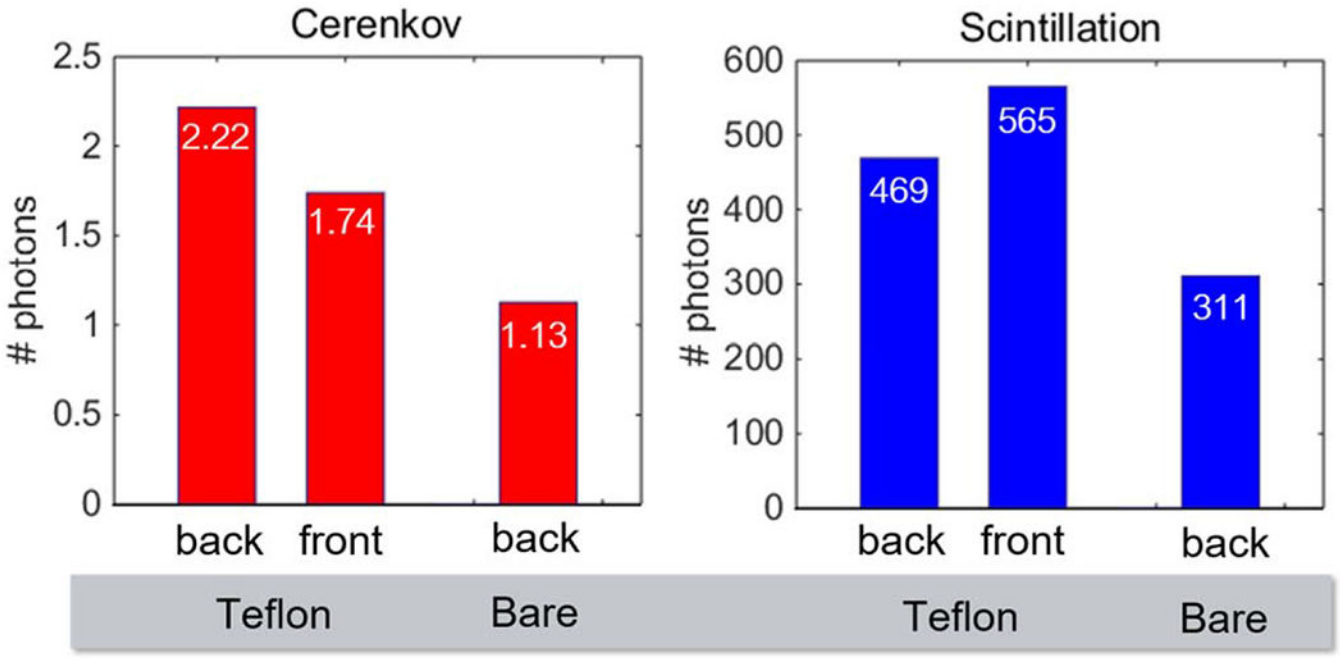


**Figure 5.**

Number of detected photons including photoelectric and Compton events. (a) Cerenkov photons. (b) Scintillation photons. For the Teflon-wrapped crystals, the photodetector was in the back or in front of the crystal. Results show that the back-to-back configuration is more favourable to the Cerenkov photons while the front-to-front configuration is more favourable to scintillation photons.

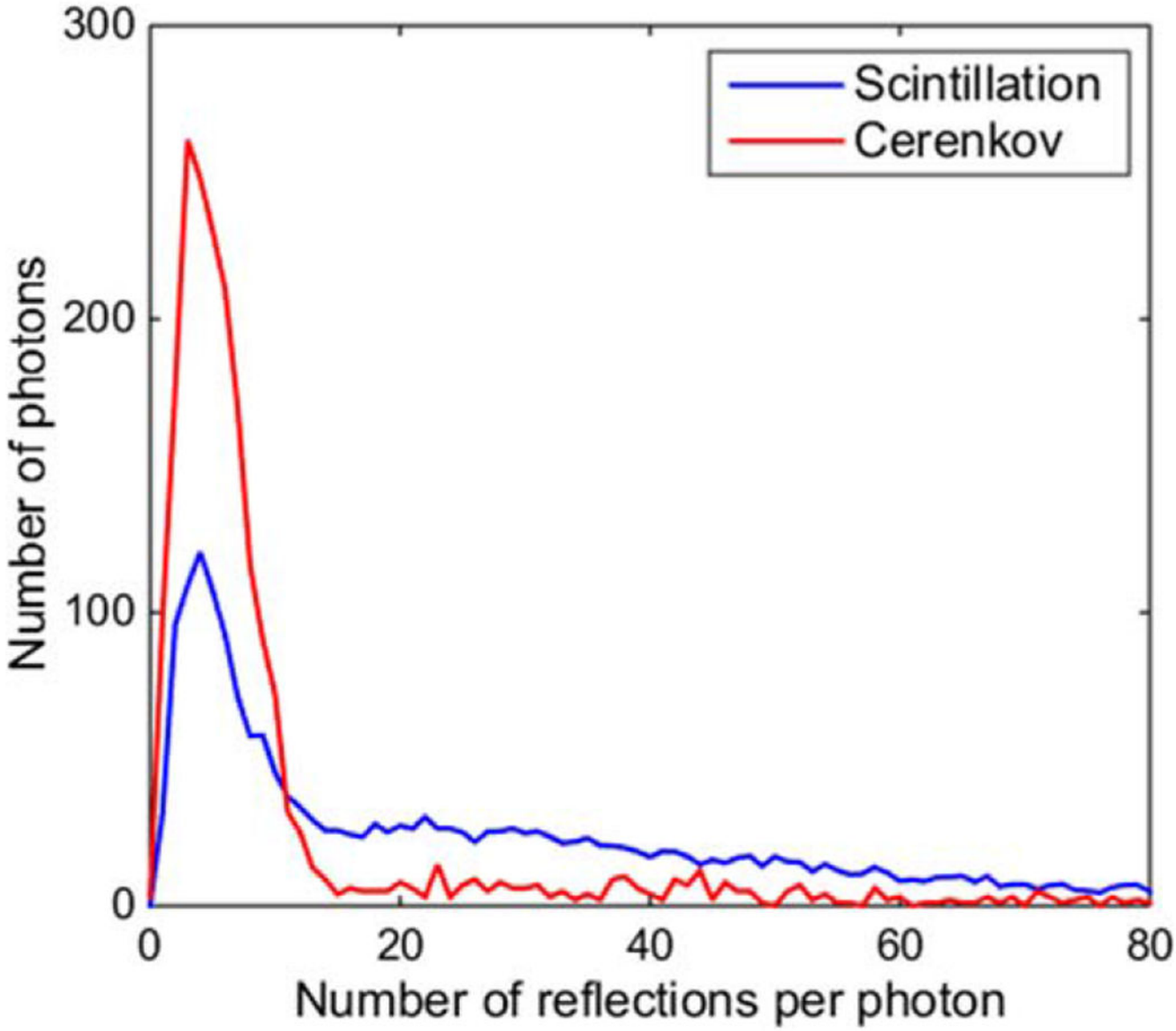


**Figure 6.**
Number of reflections per detected photon for Cerenkov and scintillation light in a 20 mm-long crystal wrapped in Teflon with the photodetector in the back.

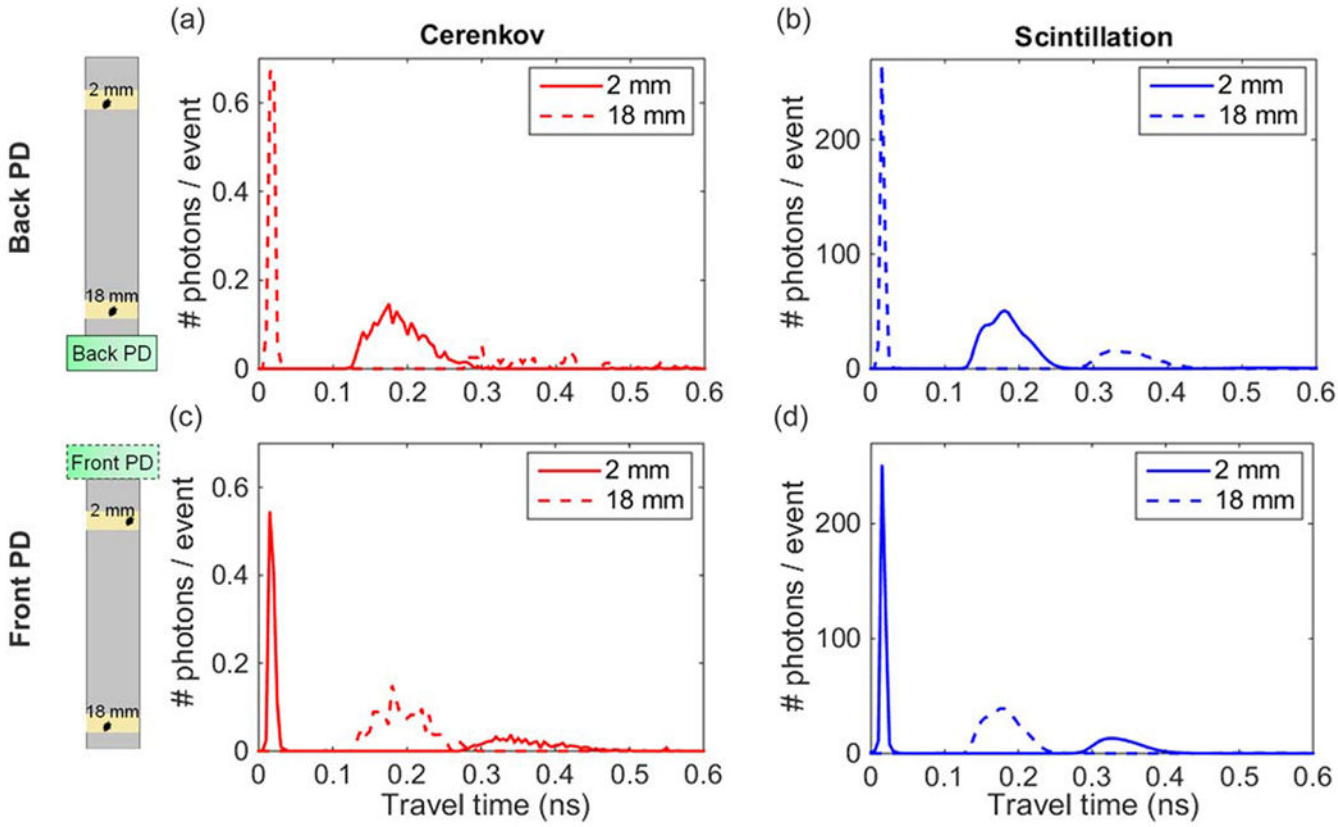


**Figure 7.**

Photon travel times for gamma interactions (represented by the black stars) at a DOI of 2 and 18 mm for a photodetector (PD) attached either to the front or back crystal face. (a) Cerenkov, Back PD (close to 18 mm). (b) Scintillation, Back PD. (c) Cerenkov, Front PD (close to 2 mm). (d) Scintillation, Front PD.

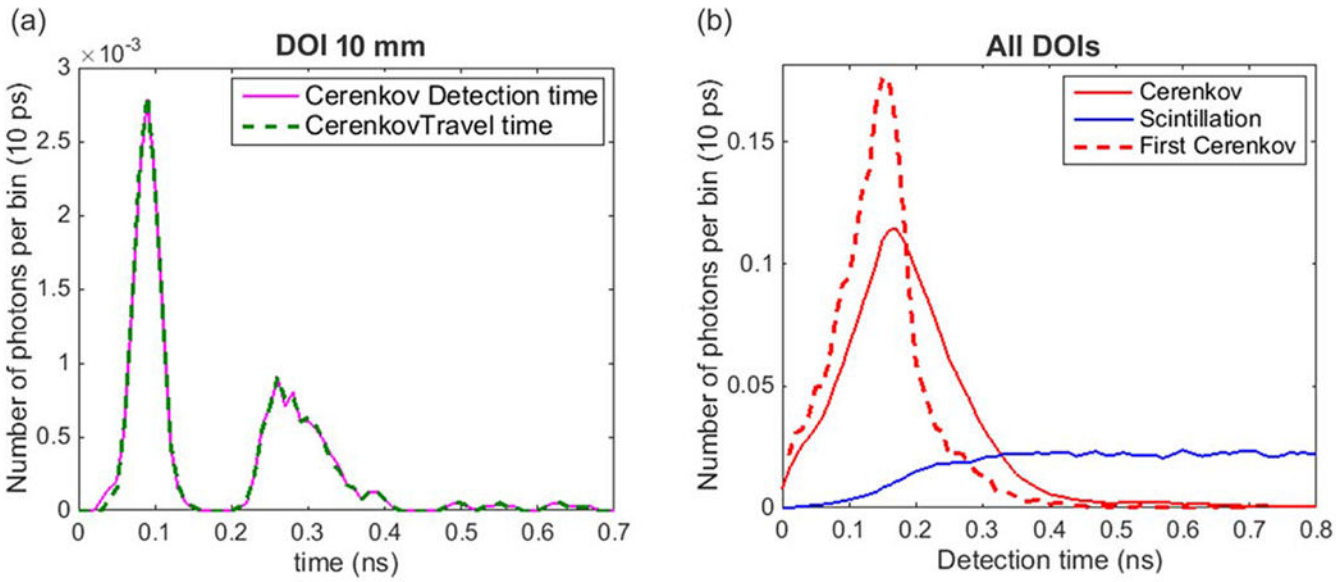


**Figure 8.**

Detail for the first nanosecond for crystal wrapped in Teflon tape with photodetector in the back. (a) Cerenkov detection and travel times for gamma interactions at DOI 10 ± 0.1 mm show a perfect match. (b) Comparison of detection times for all detected Cerenkov photons, first detected Cerenkov photon, and all scintillation photons.

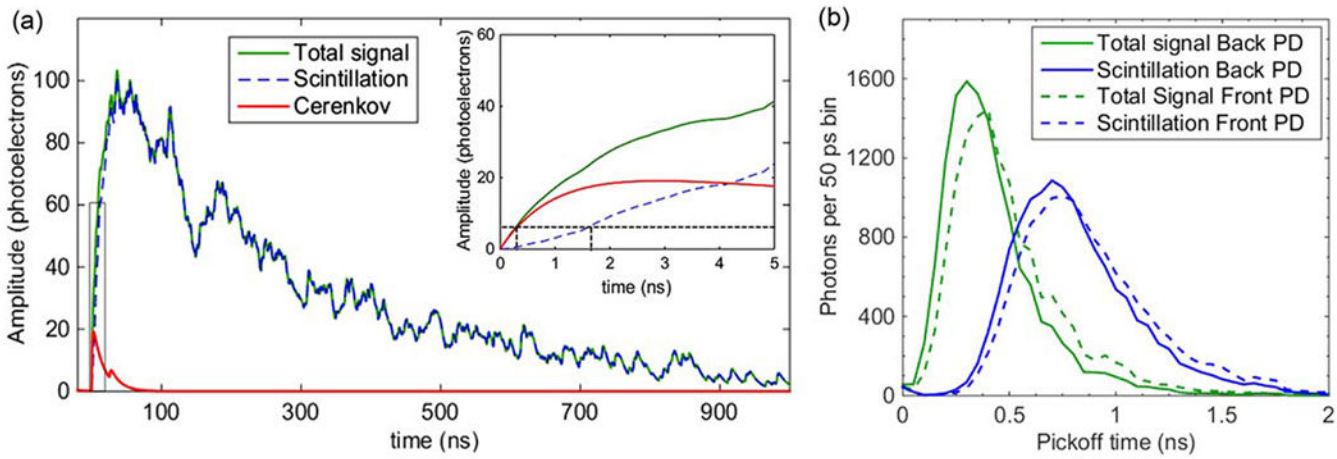


**Figure 9.**

Effect of Cerenkov photons on waveform and timing pickoff. (a) Example of waveform for a polished crystal wrapped in Teflon with photodetector in the back. Inset shows the details of the first 5 ns, with lines indicating the time the signal crosses the threshold of 5 photoelectrons. (b) The distribution of pickoff times based on leading edge is narrower when including Cerenkov photons and when the photodetector is positioned in the back.

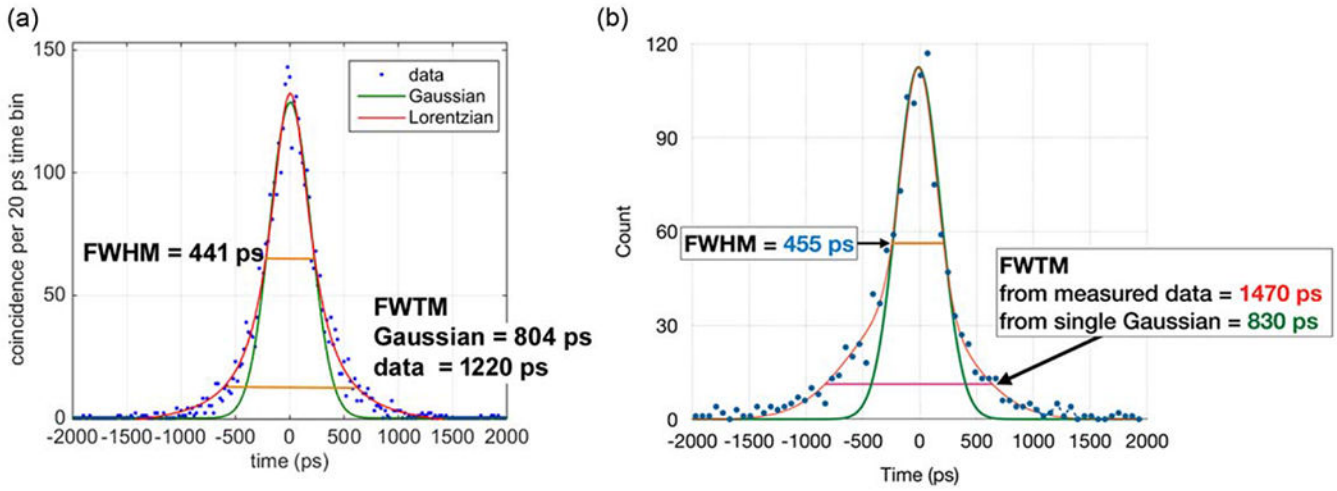


**Figure 10.**

Timing spectrum for a polished crystal wrapped in Teflon with photodetector in the back. (a) Simulated data. (B) Measured spectrum. The Lorentzian fits shows much better agreement with the simulated data distribution, confirming results observed experimentally.

**Table 1.**

Summary of detector geometries.

| | | |
|---|---|---|
| Photodetector position | Back | Front |
| Crystal surface | Polished | Polished |
| External material | No reflector (bare) | Teflon tape 5 layers |
| | Teflon tape 5 layers | |

**Table 2.**

Coincidence resolving times (CRT) for each detector configuration.

| | Total signal (with Cerenkov) | | Scintillation only | |
|---|---|---|---|---|
| | **FWHM** | **FWTM** | **FWHM** | **FWTM** |
| Polished Teflon tape back-to-back | 441 ps | 804 ps | 649 ps | 1182 ps |
| Polished Teflon tape front-to-front | 512 ps | 933 ps | 607 ps | 1106 ps |